Journal of Geochemical Exploration 149 (2015) 59–73

Contents lists available at ScienceDirect

Journal of Geochemical Exploration

journal homepage: www.elsevier.com/locate/jgeoexp

Combination of geostatistical simulation and fractal modeling for mineral resource classification

Behnam Sadeghi [a,b,*], Nasser Madani [c,d,e], Emmanuel John M. Carranza [f]

[a] Department of Mining Engineering, Faculty of Engineering, South Tehran Branch, Islamic Azad University, Tehran, Iran
[b] Young Researchers and Elite Club, South Tehran Branch, Islamic Azad University, Tehran, Iran
[c] Department of Mining Engineering, University of Chile, Santiago, Chile
[d] Advanced Mining Technology Center, University of Chile, Santiago, Chile
[e] CSIRO-Chile International Center of Excellence in Mining and Mineral Processing, Chile
[f] School of Earth and Environmental Sciences, James Cook University, Townsville, Queensland 4811, Australia

ARTICLE INFO

Article history:
Received 17 July 2014
Accepted 19 November 2014
Available online 26 November 2014

Keywords:
Mineral resource classification
SS–N model
Gaussian turning bands simulation
Fractal models

ABSTRACT

The separation, identification and assessment of high-grade ore zones from low-grade ones are extremely important in mining of metalliferous deposits. A technique that provides reliable results for those purposes is thus paramount to mining engineers and geologists. In this paper, the simulated size–number (SS–N) fractal model, which is an extension of the number–size (N–S) fractal model, was utilized for classification of parts of the Zaghia iron deposit, located near Bafq City in Central Iran, based on borehole data. We applied this model to the output of the turning bands simulation method using the data, and the results were compared with those of the application of the concentration–volume (C–V) fractal model to the output of kriging of the data. The technique using the SS–N model combined with turning bands simulation presents more reliable results compared to technique using the C–V model combined with kriging since the former does not present smoothing effects. The grade variability was classified in each mineralized zones defined by the SS–N and C–V models, based on which tonnage cut-off models were generated. The tonnage cut-off obtained using the technique of combining turning bands simulation and SS–N modeling is more reliable than that obtained using the technique of combining kriging and C–V modeling.

1. Introduction

The recognition of geochemical anomalies and their distinction from geochemical background for the identification, delineation, and modeling of mineralized zones is important in mineral exploration, mineral resource classification, and mine planning. Although various factors of mineral deposit formation control the variability in geochemical data, grades of metals in mineral deposits or concentrations of chemical elements in the Earth's crust have been assumed to follow a normal (Gaussian) or log-normal distribution in traditional statistical methods of data analysis (Armstrong and Boufassa, 1988; Clark, 1999; Limpert et al., 2001). However, many scientists and researchers have recognized and advocated that frequency distributions of element concentrations are mostly not normal (Ahrens, 1954a,b, 1966; Bai et al., 2010; He et al., 2013; Li et al., 2003; Luz et al., 2014; Razumovsky, 1940; Reimann and Filzmoser, 2000).

Geostatistical methods have been increasingly used as powerful tools for predicting spatial attributes and for modeling the uncertainty of predictions in un-sampled locations, which are important in mineral resource estimation and ore reserve evaluation (e.g., Chilès and Delfiner, 2012; Emery, 2005, 2012; Emery and González, 2007; Emery and Robles, 2009; Emery et al., 2005, 2006; Maleki Tehrani et al., 2013; Montoya et al., 2012; Ortiz and Emery, 2006). Kriging, as an important geostatistical interpolation method, is a linear and generally robust estimator, but its main disadvantage is its smoothing effect, particularly for highly skewed data. Consequently, if kriging is applied to datasets with non-Gaussian distribution, it is not able to reproduce spatial heterogeneity that is characteristic of many such datasets. In contrast, Gaussian simulation as an alternative technique for kriging provides more precise results (Deutsch and Journel, 1998; Matheron, 1973; Shinozuka and Jan, 1972), and most continuous variables can be simulated by transformation to the Gaussian (or multi-Gaussian) distribution. Gaussian simulation algorithms are divided into two types, exact and approximate algorithm (Emery and Lantuejoul, 2006). Several approximate Gaussian simulation algorithms have been developed, and one of them is called turning bands method (Matheron, 1973). It was first introduced by Chentsov (1957) in a special case of Brownian random functions, but has been extended for the Gaussian simulation of stationary and intrinsic random functions by Emery and Lantuejoul (2006) and also Emery (2008). This method aims at simplifying the

* Corresponding author.
E-mail address: behnamsadeghi.researches@yahoo.com (B. Sadeghi).

http://dx.doi.org/10.1016/j.gexplo.2014.11.007
0375-6742/

Gaussian simulation problem in multidimensional spaces, using simulations in one dimension and spreading them to 2-D or 3-D spaces. This method is extremely fast with parallelizable computations and one can simulate as many locations as desired. The Gaussian simulation also exactly reproduces the desired covariance model (Chilès, 1977; Chilès and Delfiner, 2012; David, 1977; Delhomme, 1979; Emery and Lantuejoul, 2006; Journel and Huijbregts, 1978; Mantoglou and Wilson, 1982). However, the turning bands method is like conventional geostatistical methods because it also operates on the basis of classical statistical parameters such as mean, percentile, and standard deviation and requires normalization of data that may not actually distort the real spatial distribution of geochemical data. For example, geochemical data

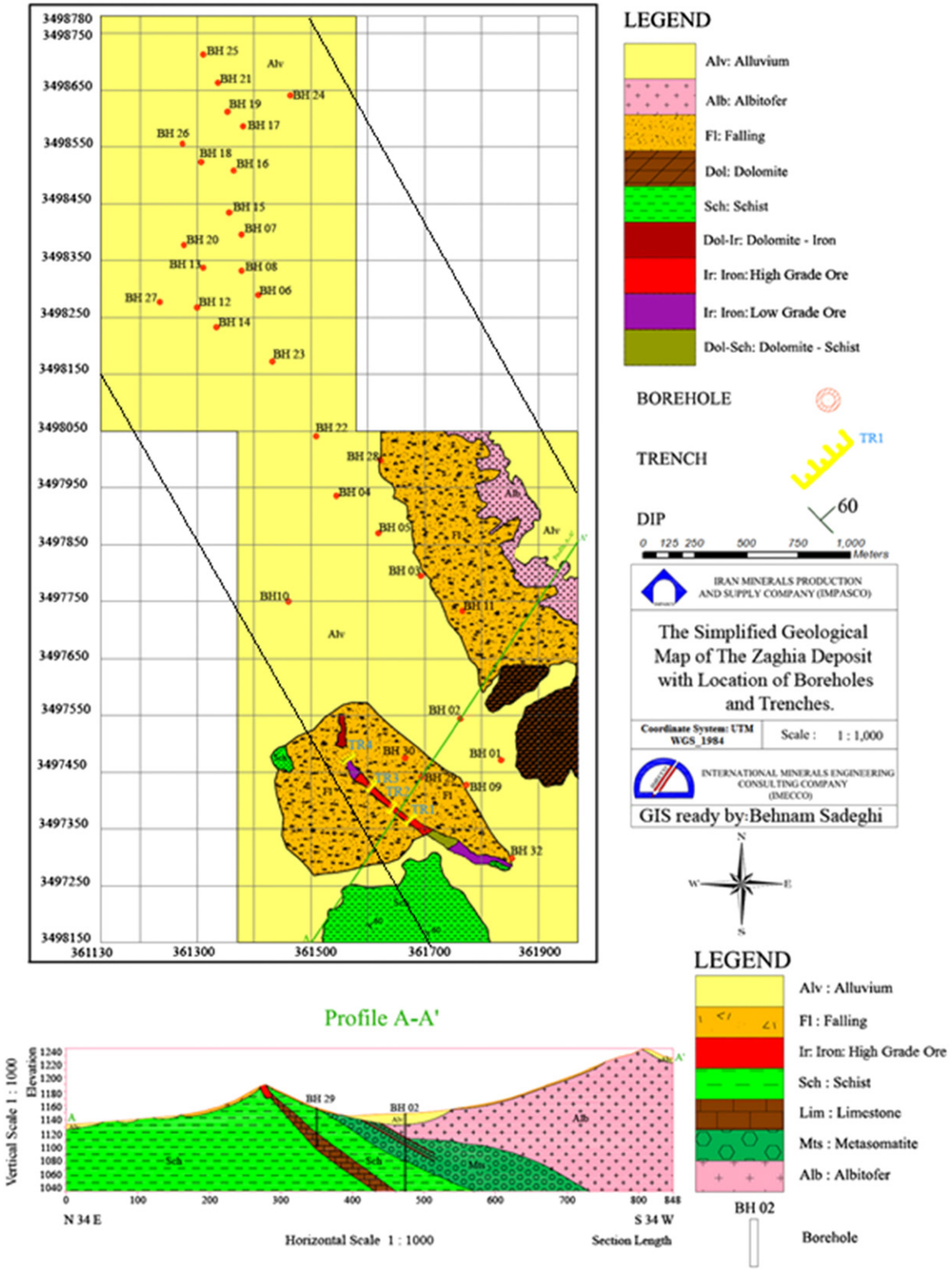

Fig. 1. Geological map of the Zaghia deposit with the locations of boreholes and trenches (from Sadeghi et al., 2012). The two slanting black lines represent boundaries of the study area.

of elements in boreholes exhibit power-law distributions that can be modeled more accurately using fractal models (Cheng et al., 1994; Monecke et al., 2001; Sanderson et al., 1994; Zuo et al., 2009).

Fractal geometry (Mandelbrot, 1983) has been applied in the geosciences since the 1980s. It is different from Euclidean geometry; whereas dimensions in the latter are whole numbers, dimensions in the former are fractions. In addition, there is a special property of 'self-similarity' in fractal geometry, which means that objects are self-similar as they are scaled down. In the past three decades, fractal geometry and fractal/multifractal models have been utilized to describe the spatial attributes of mineral deposits (e.g., Afzal et al., 2010, 2011, 2012; Carranza, 2011b; Carranza and Sadeghi, 2010; Nazarpour et al., 2015; Nouri et al., 2013; Sadeghi et al., 2012; Shen and Zhao, 2002; Turcotte, 1986, 2002; Wang and Cheng, 2006; Wang et al., 2007, 2008, 2010a,b, 2011; Zhang et al., 2001) or geochemical landscapes (e.g., Agterberg et al., 1993, 1996; Ali et al., 2007; Carranza, 2010a,b, 2011a; Cheng, 2007; Cheng et al., 1994; Goncalves et al., 2001; Sim et al., 1999; Zuo et al., 2012, 2013, 2015). In particular, the spatial distributions of chemical elements in geochemical landscapes have a fractal dimensions because they have self-similar properties in various geographic scales (Bolviken et al., 1992). The basic advantage of fractal geometry is that it considers not only frequency but also spatial

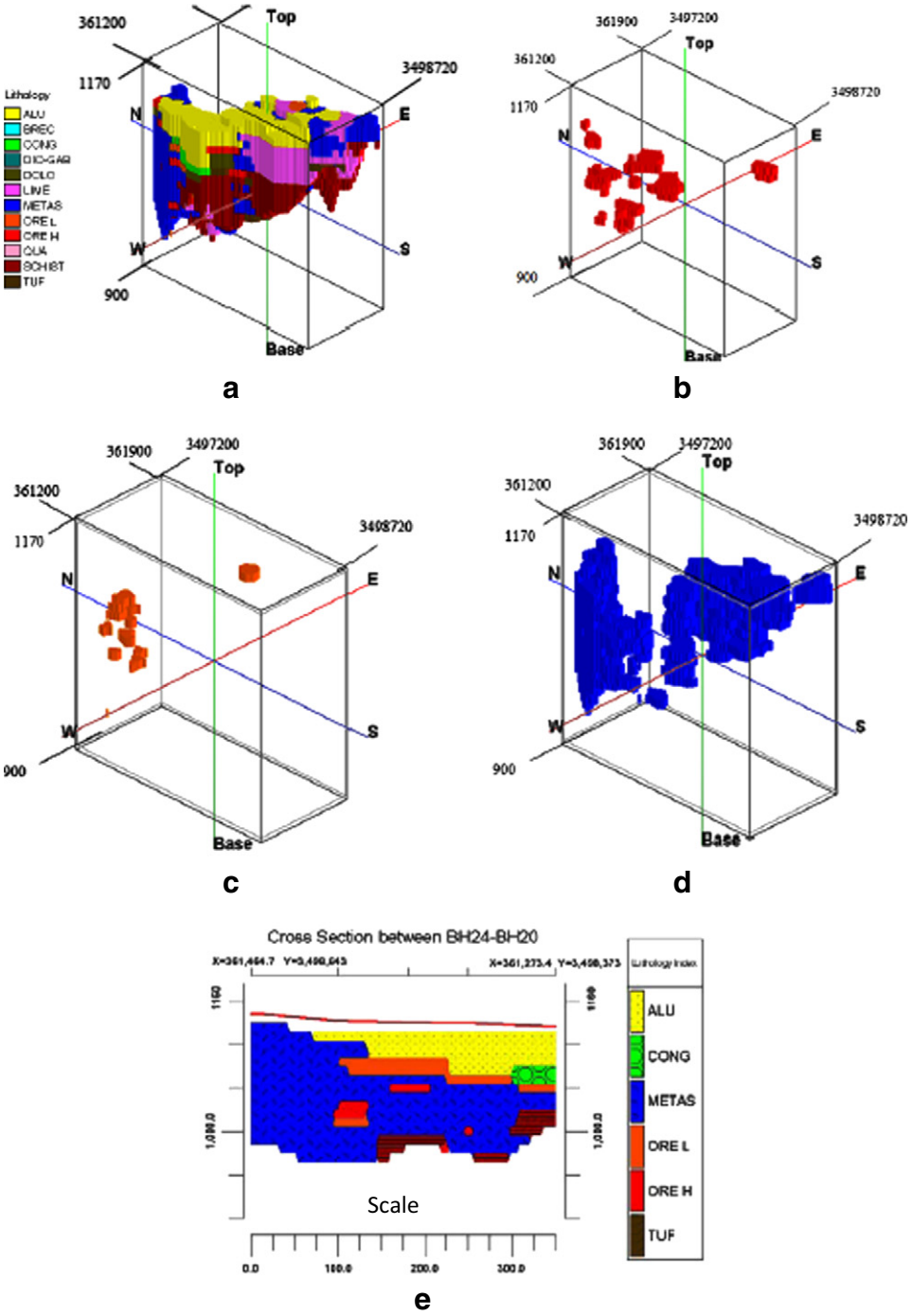

Fig. 2. 3-D models of borehole geological data in the Zaghia deposit (Sadeghi et al., 2012): (a) geological model of the deposit; (b) low grade ores; (c) high grade ores; (d) metasomatic units; (e) a representative cross-section.

distribution of data and, thus, geometrical properties of mineral deposits or geochemical landscapes (Cheng et al., 1994; Davis, 2002; Li et al., 2003).

Fractal models can be useful in solving particular problems of traditional statistical methods in exploration geochemistry, and they are based on the direct study of rocks and minerals. In general, the common problem of traditional statistical methods is that they were not developed originally for the study of distribution of chemical elements, whereas fractal models have been conceptualized for geographical as well as geological and geochemical properties that have some kind of geometrical support (Bolviken et al., 1992; Mandelbrot, 1983; Turcotte, 1986, 1996, 2002). As an example, fractal models have been used to describe and explain the spatial distribution of mineralization based on variations in geochemistry and geology through the recognition of populations in spatial data from mineral deposits (Afzal et al., 2011; Carranza, 2009; Carranza et al., 2009; Deng et al., 2010; Goncalves et al., 2001; Hassanpour and Afzal, 2011). The recognition of populations in spatial domain of data from mineral deposits through fractal analysis allows for discrimination of mineralized zones from background and for recognition of transition zones between mineralized zones with contrasting metal grades. Therefore, volumes of zones in mineral deposits can be mapped and estimated more precisely by techniques using fractal models than by traditional statistical methods. This is critical in 3-D modeling as part of quantitative assessment and prediction of mineral resources, whereby several kinds of data such as geological, geochemical, and geophysical data, with different statistical distributions, are used for exploring and delineating mineral deposits. In general, the semi-variogram as a geostatistical tool can be utilized for spatial analysis of all kinds of element distributions in mineral deposits and can provide vital parameters for interpolating, estimating and even simulating in district-scale 3-D modeling (Houlding, 2000; Wang et al., 2013; Wilson et al., 2011). However, due to the complexity of 3-D modeling and the limitations of conventional geostatistical methods discussed above, an innovative and more efficient technique is required.

In this research, an innovative technique based on the fractal theory in combination with geostatistical simulation is proposed for mineral resource classification. It can be implemented in a few steps. Firstly, Gaussian geostatistical simulation is used to reliably model the spatial distribution and spatial variability of the data. Then, the simulated size–number (SS–N) fractal model is applied to the interpolated/simulated data to determine thresholds for mapping of mineralized zones,

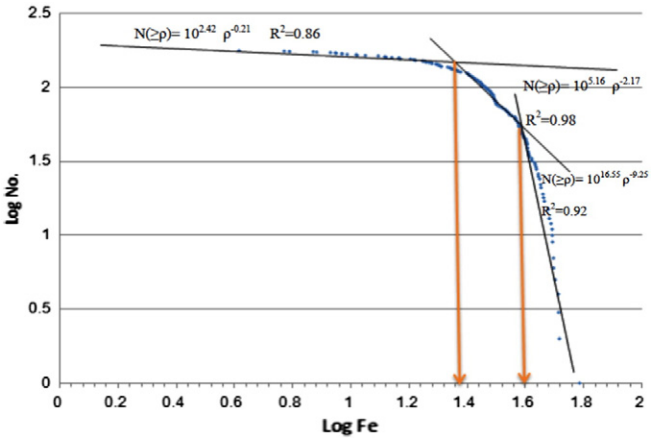

Fig. 4. N–S log–log plot for Fe concentrations in the Zaghia deposit.

which are critical for mine planning and mineral resource classifications. Mapped mineralized zones can be classified according to the classification prescribed by the Joint Ore Reserves Committee (JORC, www.jorc.org). The proposed technique combining Gaussian geostatistical simulation and SS–N fractal modeling is robust with respect to fluctuations in ore grade.

2. Methodology

2.1. Number–size (N–S) fractal model

The N–S fractal model was proposed by Mandelbrot (1983) for describing the distribution of geochemical data. According to this model, there is a relation between the number and size parameters of evaluated data. The N–S model is expressed by the following equation (Mandelbrot, 1983):

$$N(\geq \rho) = F\rho^{-D} \quad (1)$$

where ρ denotes element concentration, N(≥ρ) denotes cumulative number of samples with concentration values greater than or equal to ρ, F is a constant and D is the scaling exponent or fractal dimension of the distribution of element concentrations. According to Mandelbrot

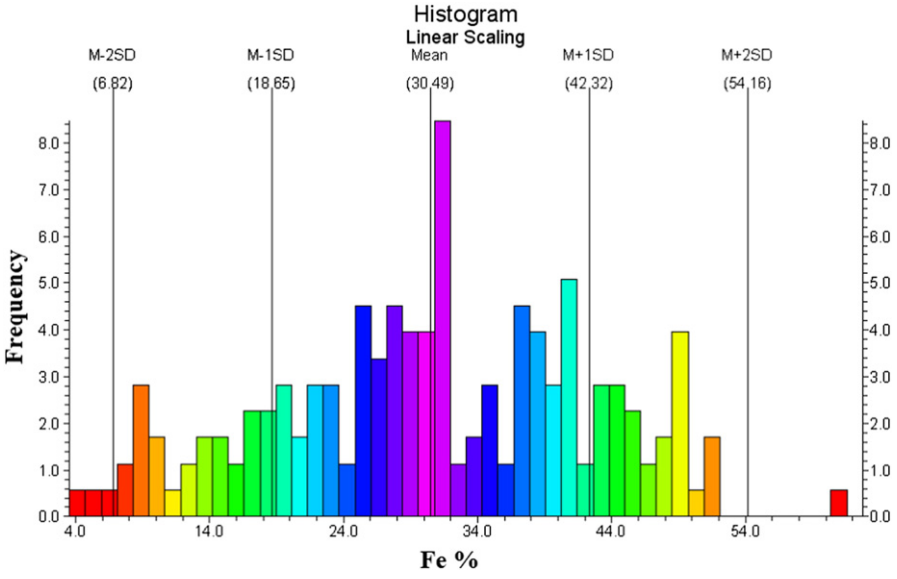

Fig. 3. Histogram of Fe concentrations in lithogeochemical samples from the Zaghia deposit.

Table 1
Zones in the Zaghia deposit based on two thresholds of Fe contents defined by the N–S fractal model.

Mineralized zones	Range Fe%
Wall rocks and weakly mineralized	<23.9
Moderately mineralized	23.9–39.8
Highly mineralized	>39.8

(1983), log–log plots of $N(\geq\rho)$ versus ρ show straight line segments with different slopes — D corresponding to different concentration intervals.

Agterberg (1995) proposed a 'concentration–size' multifractal model based on the N–S model in order to determine and describe the spatial distribution of geochemical attributes in large mineral deposits. Monecke et al. (2005) used the N–S model to describe geochemical data, which indicate enrichment of minerals by replacement due to metasomatic processes resulting in the formation of hydrothermal deposits in the Waterloo massive-sulfide deposit, Australia. The power-law frequency model, which has been suggested based on the N-S model, measures the frequency distribution of element and mineral concentrations based on the number of samples (Li et al., 1994; Sadeghi et al., 2012; Sanderson and Zhang, 1999; Shi and Wang, 1998; Turcotte, 1996; Zuo et al., 2009). The first 3-D modeling work based on the N–S fractal model was demonstrated by Sadeghi et al. (2012) for the separation of mineralized zones and wall rocks, and the precision and thus the applicability of the model was proven by comparison of results with those of the concentration–volume (C–V) fractal model. The most important advantage of this model is that there is no need for pre-processing of data for pre-estimation before modeling.

2.2. Turning bands simulation

This method aims at simplifying the Gaussian simulation problem in multi-dimensional spaces, using simulations in one dimension and "spreading" them to 2-D or 3-D space, thus (Chilès and Delfiner, 2012):

$$Y(x) = Y^{(1)}(\langle x|u\rangle) \tag{2}$$

where $Y^{(1)}$ is a random function in 1-D space, and U is a vector in multi-dimensional space and $\langle x|u\rangle$ is a location x projection on the extended line with a U vector.

For displaying the relationship between covariance functions in 1-D and 2-D space, we can let C_1 be the covariance of $Y^{(1)}$ and C_d, the covariance of $Y(x)$, can be defined as (Brooker, 1985; Gneiting, 1998; Lantuejoul, 2002; Matheron, 1973):

$$C_d(h) = C_1(\langle h|u\rangle) \tag{3}$$

This covariance becomes isotropic if one draws the direction of u at random, i.e., if one replaces the deterministic vector u by an isotropic random vector U, thus:

$$C_d(h) = E\{C_1(\langle h|u\rangle)\} \tag{4}$$

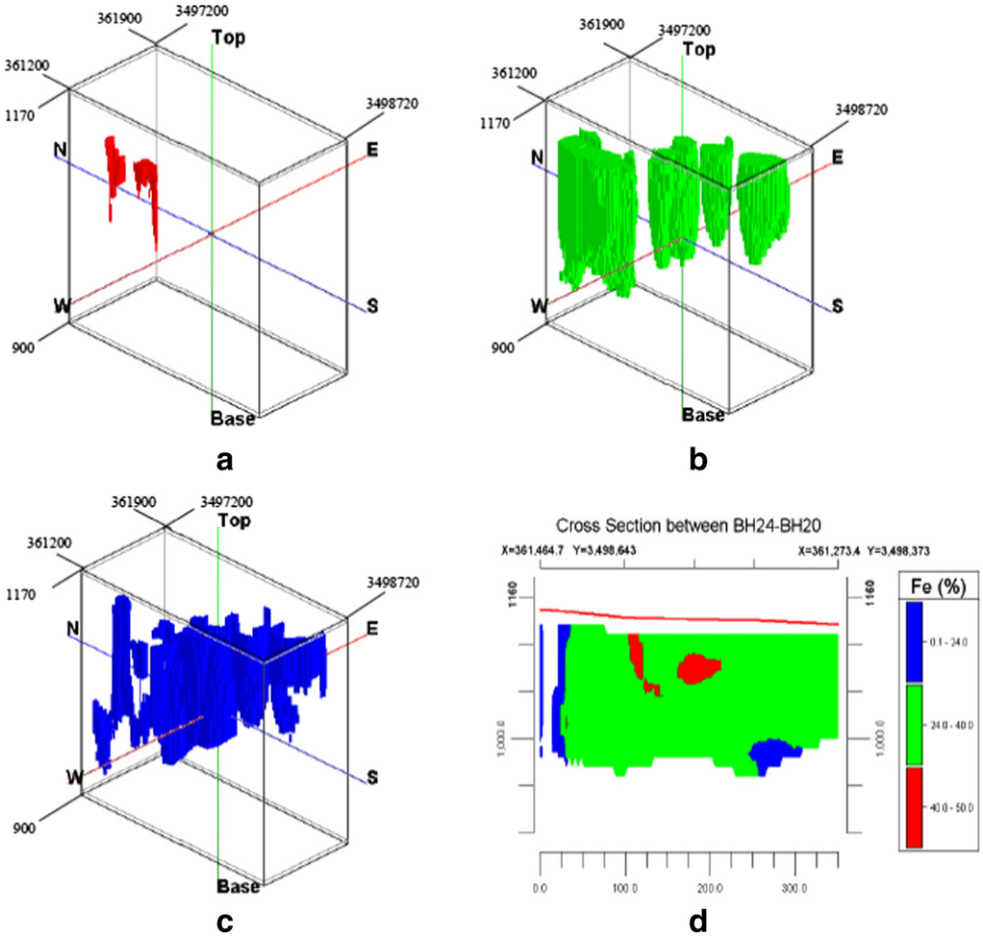

Fig. 5. Classified zones based on thresholds defined using the N–S fractal model of Fe data (Sadeghi et al., 2012): (a) highly mineralized zones; (b) moderately mineralized zones; (c) weakly mineralized zones and wall rocks; and (d) a cross-section of the mineralized zones.

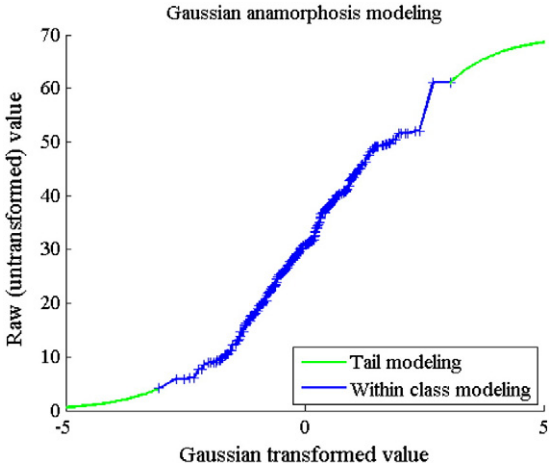

Fig. 6. Gaussian anamorphosis modeling.

The mapping $C_1 \rightarrow C_d$ is one-to-one, so that one can simulate a multi-dimensional random function with covariance C_d by means of a 1-D random function with covariance C_1 and a random direction, which is defined in the spreading process. The transition of covariance from 1-D to 3-D spatial domain can be simplified as follows (C_2 and C_3 are C_d for $d = 2$ and $d = 3$, respectively):

$$C_1(r) = \frac{d}{dr}[rC_3(r)] \tag{5}$$

and the covariance transition from 1-D to 2-D is more complex, thus:

$$C_1(r) = \frac{d}{dr}\int_0^r \frac{t}{\sqrt{r^2 - t^2}} C_2(t)dt \tag{6}$$

For obtaining a multi-Gaussian random and ergodic functions, it is required to calculate the average of the independent simulations as follows:

$$Y(x) = \frac{1}{\sqrt{N}}\sum_{i=1}^{N} Y_i^{(1)}(\langle x|u_i\rangle) \tag{7}$$

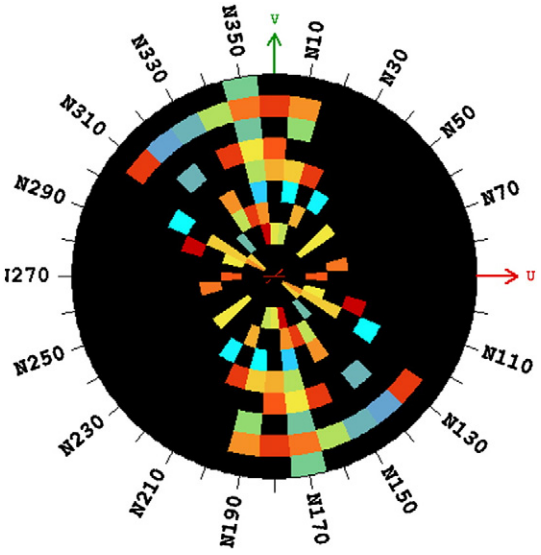

Fig. 7. 2-D plot of the sample variogram for all experimentally variable separation vectors, depicting colors varying from blue (low value) to red (high value) and representing inconsistency or variability of anisotropy.

Obtaining a multi-Gaussian random field requires numerous lines in 1-D space, and that means that the simulated random function is not multi-Gaussian. To speed up the convergence to the multi-Gaussian distribution, it is advisable to use equi-distributed directions and to consider several hundreds or thousands of directions (Emery and Lantuejoul, 2006).

2.3. Turning bands simulated size–number (SS–N) fractal model

The proposed technique of combining turning bands simulation and SS–N fractal model is a geostatistical extension of the N–S model based on the combination of geostatistical simulation and fractal/multifractal modeling. We propose to relate simulated size (SS) and number (N) of evaluated data with the following equation:

$$N(SS \geq \rho) = F\rho^{-D} \tag{8}$$

where ρ denotes element concentration, $N(\geq\rho)$ is cumulative number of samples with the average of the simulated concentration values greater than or equal to ρ, F is a constant and D is the fractal dimension of the distribution of element simulated concentrations. With this model, one generates a large number of realizations by any type of multi-Gaussian simulation approach (preferably, turning-bands). The various realizations generated are comparable in their spatial variability. The most significant issue is to produce "alternative realities" phenomena, which are legitimately flexible to the fluctuations of the underlying statistical parameters. This could be an excellent alternative for some other approaches that produce just one realization (Chilès and Delfiner, 2012). Whereas kriging is generally the best interpolation method, it is not able to produce interpolated data with the same spatial variability as the given original data, unless the data have a strictly Gaussian distribution.

The realizations generated by the proposed technique mimic the spatial variability of the given original data. A meaningful application of the proposed technique is to evaluate ore reserves and estimate mineral resources. The separation of mineralized zones is particularly crucial for the estimation of mineral resources. One can implement the following steps to first map mineralized zones and then classify mineral resources with focus on handling spatial uncertainty.

Step 1 N–S modeling
Step 2 Spatial data analysis
Step 3 Geostatistical simulation
Step 4 SS–N modeling
Step 5 Mineral resource classification

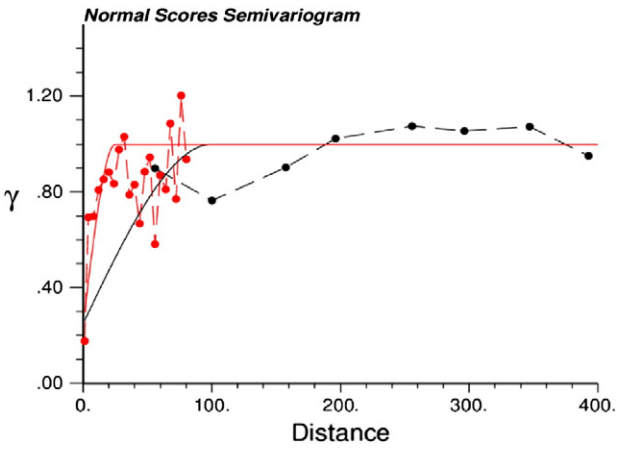

Fig. 8. Normal scores semi-variogram. Sill = 1; horizontal range = 100; vertical range = 75; nugget effect = 0.25.

3. Application to the Zaghia iron ore deposit

The Zaghia iron ore deposit, anomaly 2C, is located 120 km east of Yazd and 15 to 17 km east of Bafq in the Yazd province, and it is situated within the area covered by the Esfordi 1:100,000 scale map sheet of Iran. From a topographic point of view, the region where the deposit exists consists of two parts, (i) Quaternary alluvial sediments and (ii) semi-mountainous areas. The sediments are cut by drainage channels with the NW–SE and NE–SW trends. The anomaly 2C is limited by mountains to the east. It is located 12 km south-east of the Choghart iron mine (Fig. 1). The Zaghia iron ore deposit occurs either as a shallow outcrop or a concealed resource. Most of the anomaly is covered by alluvial sediments and only a small outcrop of iron ore is visible in the eastern area.

The Zaghia deposit is a Kiruna-type Fe–P oxide deposit, which is the same type to which the Choghart, North Anomaly and Mishdavan iron ores belong (IMECCO, 2010). It is one of the Fe deposits hosted by a sequence of pre-Cambrian and Cambrian rhyolitic volcanic rocks with intercalated shallow-water sedimentary rocks. The stratabound and zoned ore deposit has a significant Fe-oxide-rich core and an overlying body of breccia and metasomatite that is rich in hematite and magnetite. There are three principal paragenetic stages of apatite mineralization. These stages are mainly associated with Fe-oxide-rich (magnetite) ore or metasomatic Fe-poor ore characterized by vein-style accumulation of pyrite and hematite (Ramezani and Tucker, 2003; IMECCO, 2010; Sadeghi et al., 2011, 2012). Some outcrops of metasomatic units exist in the northern and southern parts of the deposit (Fig. 2). Detailed exploration of the deposit was carried out by IMPASCO, and it includes 31 exploration boreholes and four trenches.

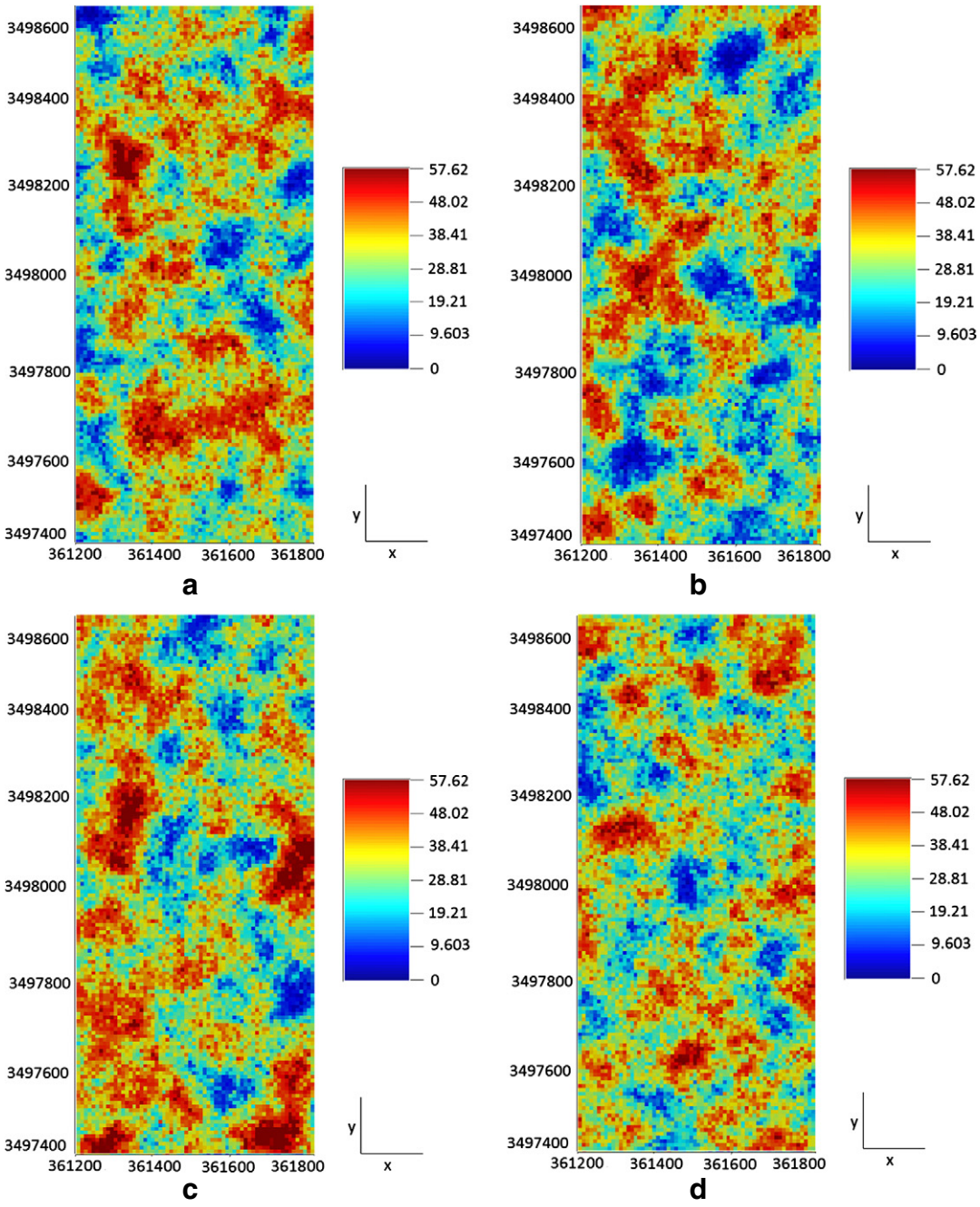

Fig. 9. Results for different numbers of realizations: (a) 20; (b) 40; (c) 60; (d) 80.

For this study, 177 lithogeochemical samples were collected at 2 m intervals along 19 boreholes in the deposit. The samples were analyzed by XRF for a number of elements related to Fe mineralization; however, only Fe data were evaluated in this study. The histogram of the Fe data shows a multi-modal distribution with a mean value of 30.49% Fe (Fig. 3).

3.1. Step 1: N–S modeling

Fractal models have been often used for characterization, delineation and separation of mineralized zones and have been seldom used for estimation of mineral resources (e.g., Wang et al., 2010a,b, 2011, 2012). However, fractal models can be applied to 3-D mineral resource estimation as well. The importance of fractal models is their better ability for the separation of mineralized zones because with conventional statistical methods researchers attempt estimation after normalization of the data whereas with fractal models there is no need for normalization of data, but they can provide more reliable estimates of mineral resource. For instance, pre-estimation results obtained by any geostatistical methods, such as kriging, always contain errors that can propagate and become compounded in the final estimation using another method. In addition, Sadeghi et al. (2012) proved that this method can yield better and more detailed results than the C–V model, which is one of the most important fractal models used for 3-D analysis, especially in cases of irregular grids of boreholes. Moreover, Sadeghi et al. (2011) and Daneshvar Saein et al. (2013) proposed this method for modeling of vertical distributions of elements in boreholes, and they proved that this method is a useful means for accurate modeling of shape of deposits.

To avoid propagation error from a pre-estimation step and to obtain accurate results, the N–S fractal model was utilized as it does not need any pre-estimation procedure as in the application of the C–V model (Sadeghi et al., 2012). In the N–S log–log plot (Fig. 4), threshold values obtained are breakpoints of straight lines fitted through least-square regression (Agterberg et al., 1996; Spalla et al., 2010). Based on the N–S model, the fractal dimensions are the slopes of individual line segments, which also indicate intensity of element enrichment (Afzal et al., 2010; Bai et al., 2010). Hence, there are three populations in the Fe data. The first Fe threshold is 23.9%, and values of <23.9% Fe are related to wall rocks and weakly-mineralized zones (Table 1). The second Fe threshold is 39.8%, and values of 23.9–39.8% Fe are related to moderately-mineralized zones (a combination of low and high grade ores), whereas values of >39.8% Fe are related to highly-mineralized zones (magnetite ore). Therefore, based on the 3-D classification of the Fe data using the

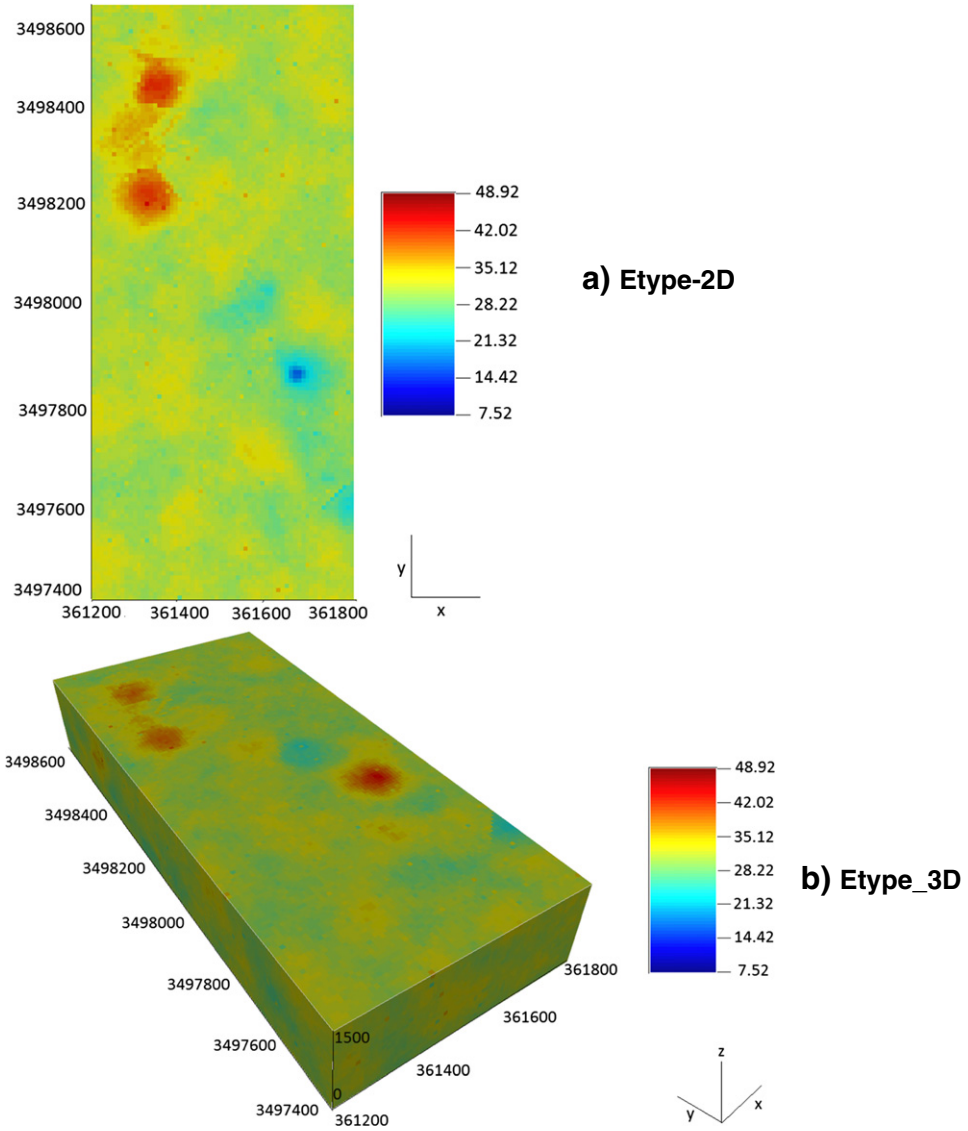

Fig. 10. E-type models (2-D and 3-D) obtained from 100 realizations.

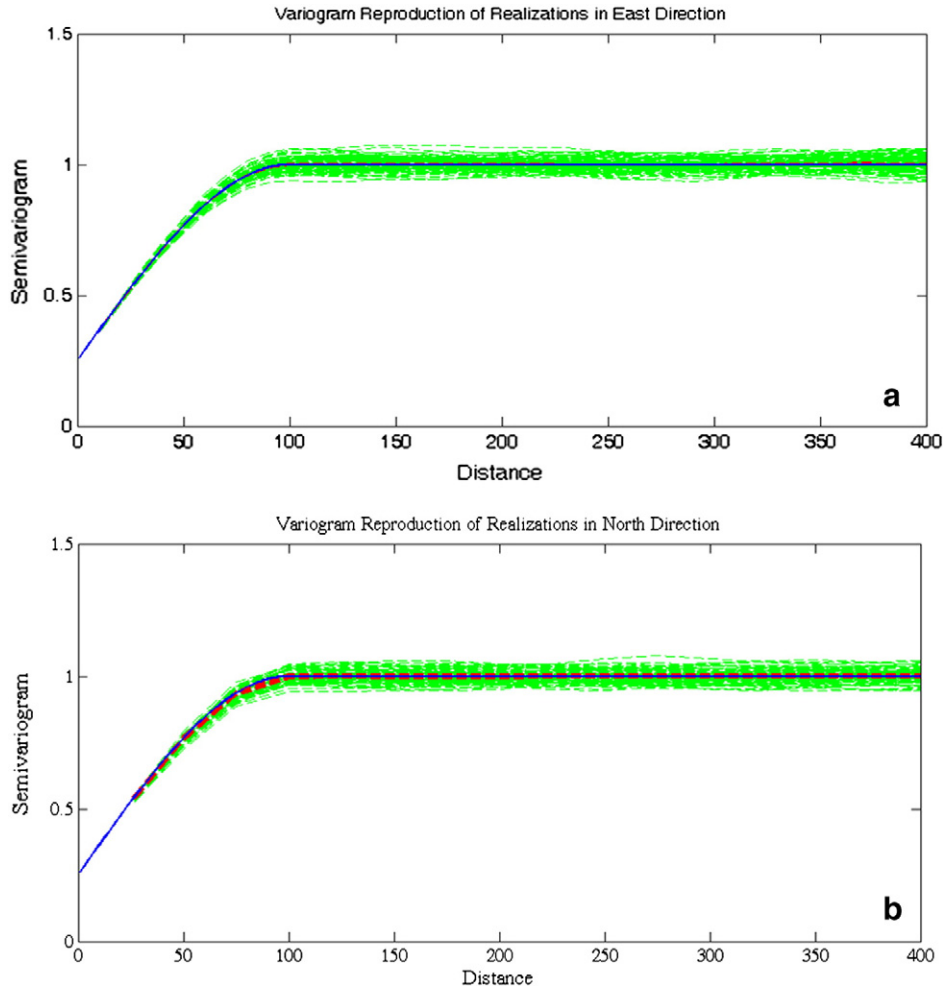

Fig. 11. Variogram reproductions of realizations in (a) east direction and (b) north direction. Green: experimental variogram of 100 realizations. Red: average of 100 realizations. Blue: theoretical model of the declustered primary data.

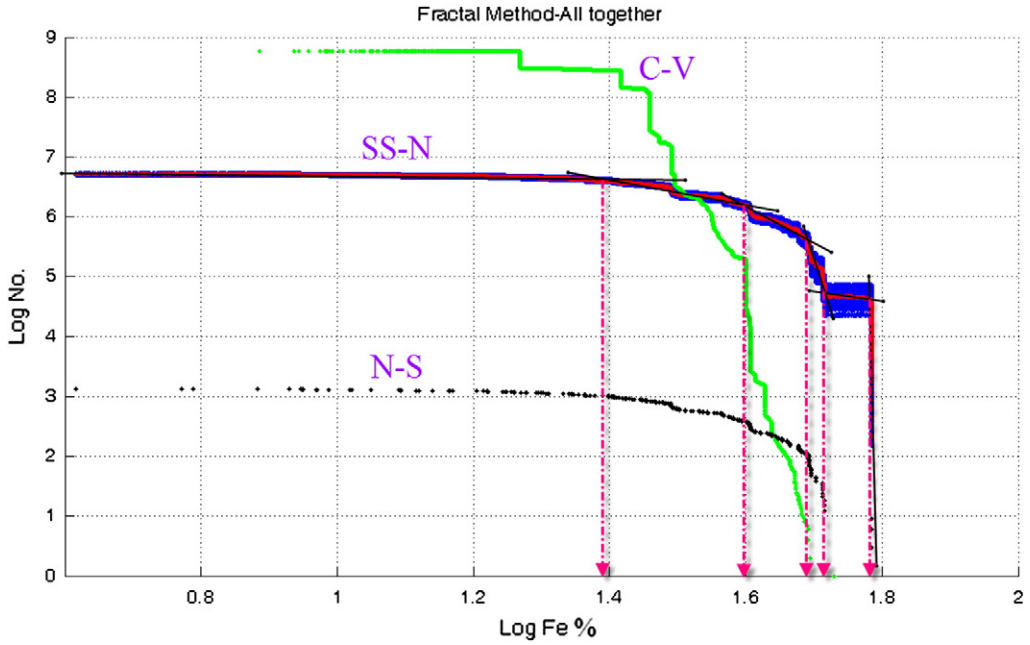

Fig. 12. Comparison of results of all methods, and the thresholds defined using the SS–N model.

Table 2
Comparison between kriging and simulation.

	Min	Max	Mean
Original data	4.13	61	30.26 (declustered)
Kriging	8.97	47.14	30.93
Simulation	1.83	66.27	30.92

thresholds obtained from the application of the N–S fractal model, highly-mineralized zones are situated in the northern part of the deposit (Fig. 5a), moderately-mineralized zones follow a NW–SE trend (Fig. 5b), and weakly-mineralized zones and wall rocks are situated in the margins of the deposit (Fig. 5d).

3.2. Step 2: spatial data analysis

As a general rule, mineral resource simulation requires suitable statistical tools for better investigation of spatial distribution. However, borehole spacing is seldom regular and may be concentrated in high grade areas. Therefore, a declustering technique is needed to provide representative distribution of the underlying attributes in a region. Such technique assigns a weight to each location based on closeness to surrounding data. Subsequently, we used a cell declustering method (Journel, 1983; Deutsch and Journel, 1998) for the composited Fe data.

Some geostatistical methods are sensitive to the presence of trends in the variability of ore grades (Rossi and Deutsch, 2014). Therefore, in the second stage, it is crucial to detect possible trends in different directions (i.e., easting, northing, and elevation). However, results of trend analysis indicate that there is no drift in the Fe data and, thus, the hypothesis of stationary can be honored in the geostatistical simulation process.

For spatial data analysis, it is common to transform data to approximate Gaussian distribution. Likewise, modeling of prediction uncertainty at un-sampled locations by Gaussian simulation requires that data are standardized to obtain normally distributed values. In this study, a Gaussian anamorphosis function is used to transform the Fe data into a Gaussian variable with mean 0 and variance 1. In this approach, one constructs the sample cumulative histogram by applying declustering weights. As a result, it is necessary to interpolate and extrapolate the cumulative histogram of the original data (Chilès and Delfiner, 2012). The lower and upper tails are correspondingly set to 1 and 0.95 as shown in Fig. 6 to get the simulated results close to actual values after back-transformation. Lastly, the procedure as described predicts the quantitative spatial variability or continuity by semi-variogram analysis. Continuity is a measure of geological properties against distance, which can be sensitive to the different directions as in mineralization systems. The form of spatial variability in mineralization systems is so-called anisotropic behavior because there is more continuity in one direction than in others. A variogram map (Deutsch and Journel, 1998), which is a 2-D plot of the sample variogram for all experimentally variable separation vectors, was generated to understand the anisotropy of Fe in the region (Fig. 7). This is a global view of the variogram values in all directions. The value $(0) = 0$ plots at the center of the figure. The horizontal values of variogram plot as colorscale at offset $h = 100$ from that center. The other black pixels which are not filled by the experimental values are left uninformed. As can be seen, one cannot distinguish a sensible direction of anisotropy in the plane. Therefore, it can be concluded that the variogram in the plane is isotropic. In order to check the anisotropy direction in vertical elongation, several variograms were calculated with over 22.5° of tolerance and showed minor anisotropy in about 90° vertical. The semi-variogram equation can be presented as follows (Fig. 8):

$$\gamma(h) = 0.25 + 0.75 \quad \mathrm{Sph}(100, 100, 20) \tag{9}$$

where 0.25 is nugget and the sill is 1 (Gaussian data), ranges 1 and 2 in the plane are both 100 m (the same in all directions of the plane) and range 3 is 20 m according to the vertical elongation, Sph provides the spherical model.

3.3. Step 3: geostatistical simulation

The turning bands simulation is implemented by the TBSIM program provided by Emery and Lantuejoul (2006) with a MATLAB source code. A regular 3-D grid with the $10 \times 10 \times 12$ m^3 block support is utilized for this study. One hundred realizations and thousand lines were produced including ordinary kriging (OK) with a search radius of 500 m in horizontal directions and 100 m in vertical directions. Because the Gaussian simulation produces equi-probable scenarios from the spatial variability, all the realizations have similar statistical properties with the legible fluctuations. Here, to illustrate the results, the realizations #20, #40, #60 and #80 were selected randomly for the 7th mine level because this is the most important level of Fe concentration (Fig. 9), and an E-type map obtained from block averaging of 100 realizations is shown as well (Fig. 10).

Validation of the output of a Gaussian simulation algorithm is performed by comparing variograms of a set of realizations with the variogram of a theoretical model. However, differences between the realization parameters and the theoretical model parameters are ideally

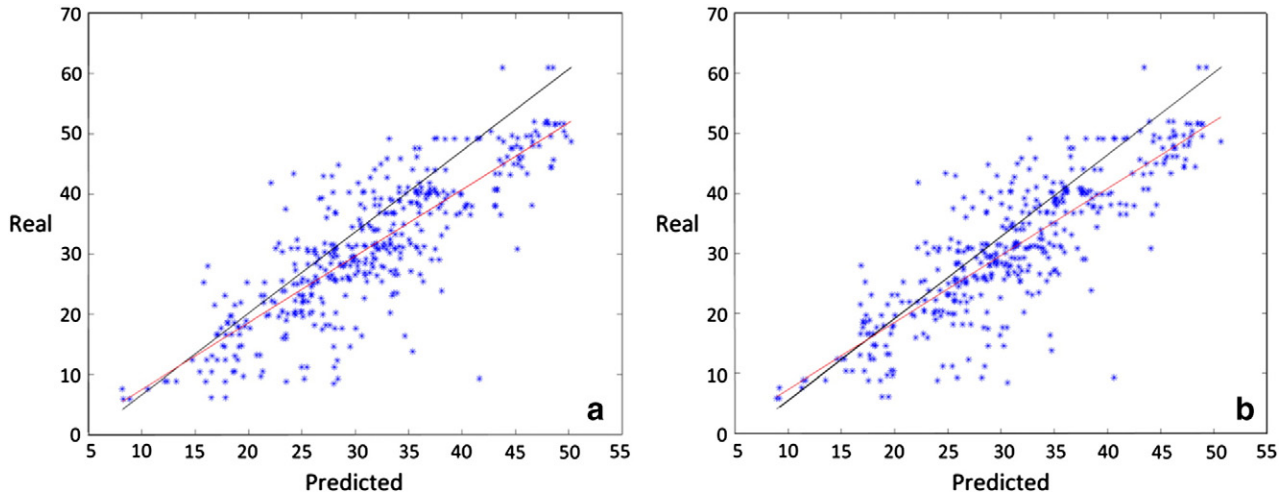

Fig. 13. Cross-validation for (a) kriging and (b) simulation. Red: regression. Black: diagonal lines.

Table 3
Cross-validation specifications.

	Intercept	Slope	Correlation Coefficient
Kriging	3.77	1.11	81.28 (%)
Simulation	3.53	1.10	82.03 (%)

typically owing to the bounded region used in Gaussian simulation processes (Matheron, 1989). If the variogram of a realization does not match that of a theoretical model, it reflects that the Gaussian simulation algorithm does not work properly. The comparison with the theoretical model should be done only after averaging the regional statistics over a large number of realizations (Emery, 2004). Hence, the variograms of the 100 realizations are compared with the variogram model and the results indicate a superb reproduction (Fig. 11).

3.4. Step 4: SS–N modeling

After generating the final simulated models (100 realizations) and the respective N–S log–log plots, the average of all log–log plots for the 100 realizations was calculated and six straight line segments have been fitted through the averaged graph of the realizations. Five thresholds were obtained at 24, 40, 50, 52.5 and 60% Fe. Compared to Fig. 12, it can be seen that there is a satisfactory correspondence between the SS–N and N–S log–log plots. However, the SS–N plot is more enhanced and structured, as it separates populations more precisely. To complete the evaluation of the SS–N model, a C–V plot was also created. The points on the C–V plot were found biased with respect to the geological concept of the ore deposit. In regard to the efficiency of the proposed approach, it was presented earlier that the simulation is able to reproduce the spatial variability and global uncertainty whereas kriging suffers from smoothing effect (Table 2). However, cross-validation is needed to reflect the goodness of fitting between the estimated or simulated and real attributes (Deutsch and Journel, 1998). In cross-validation technique, actual data are removed one at a time and re-estimated based on remaining neighborhood data. Each data attribute is replaced in the data set once it has been re-estimated or re-simulated. As can be seen from Fig. 13, both Gaussian simulation and kriging show satisfactory results and the correlation coefficient is somewhat analogous (Table 3). However, the C–V model inherits the smoothness and the under- and over-estimation errors obtained from kriging particularly the tail and head of the C–V curve have been drastically reduced and increased, respectively, although the cross-validation shows satisfactory estimation by kriging. It can be deduced that the thresholds obtained from the SS–N modeling are more trustworthy than those from the C–V modeling. For instance, the generated SS–N

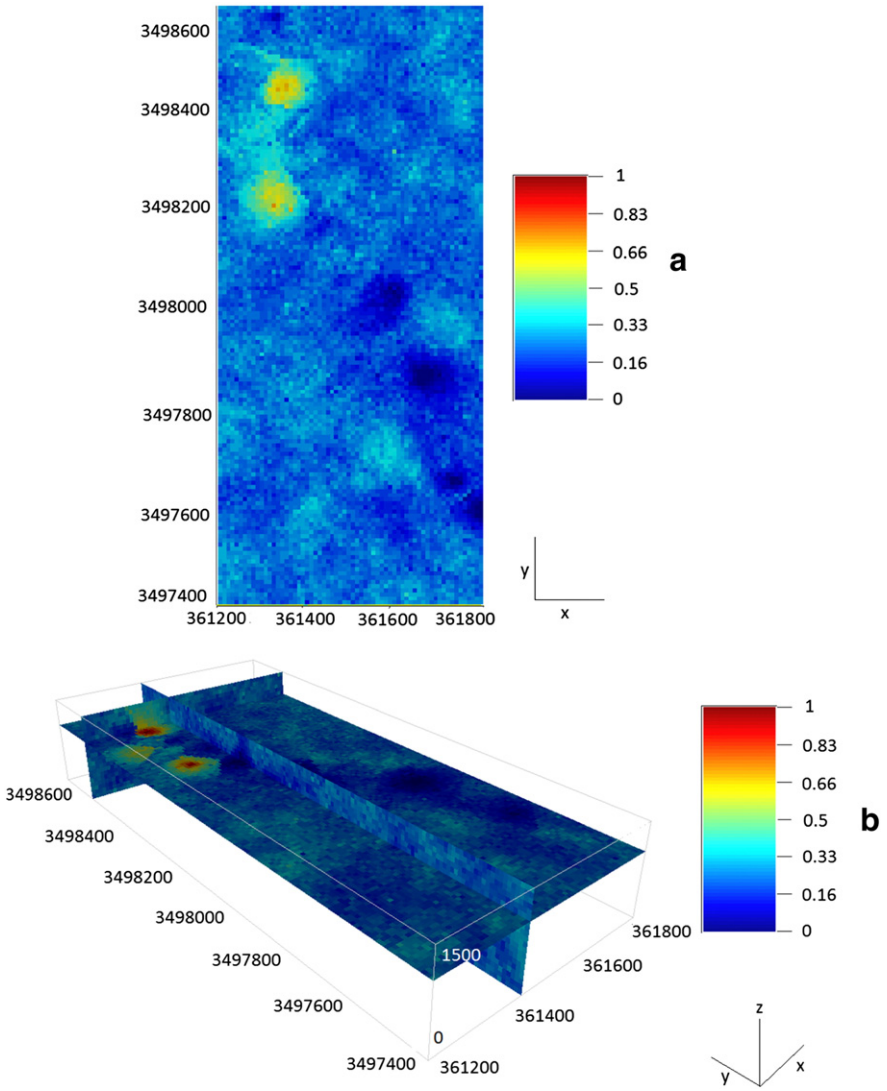

Fig. 14. Probability above threshold 40% in (a) 2-D and (b) 3-D.

Table 4
Mineral resource classification.

%	Zone	Measured			Indicated			Inferred			Total Tonnage
		Metal quantity (Mt%)	Tonnage (Mt)	Mean grade (%)	Metal quantity (Mt%)	Tonnage (Mt)	Mean Grade (%)	Metal quantity (Mt%)	Tonnage (Mt)	Mean grade (%)	(Mt)
<24	Wall rocks	68	3.081	22.07	915.210	40.399,236	22.65	1608.1	93.271	17.22	136.850
24–40	Weakly mineralized zones	9192.5	295.840	31.07	2227.6	64.066	34.76	257.870	6.722,900	38.35	366.630
40–50	Low grade zones	43.783	1.024	42.72	455.280	11.118,000	40.94	3490.1	79.302,078	44.00	91.444
50–52.5	Moderately mineralized zones	0.829700	0.16297	50.90	1.007,300	19.732	50.98	208.530	4.083,800	51.06	4.119,800
52.6–60	Highly mineralized zones	0.139500	0.002624	53.05	0.526390	0.0097524	53.76	122.100	2.242300	54.44	2.254,700
>60	Riched zones	–	–	–	–	–	–	2.622,100	0.042,800	61.11	0.042,800
										Sum	601.341,300

curve is consistent with the maximum and minimum values of the global distribution, indicating its high level of capability and performance. Subsequently, the local uncertainty can be modeled by probability plots above each threshold for application in the mine planning process. For instance, the uncertainty above threshold 40% is presented in Fig. 14.

3.5. Step 5: mineral resource classification

Mineral resource classification is crucial in uncertainty assessment and risk analysis for mineral resource development. An important feature of the SS–N model in mineral resource classification is its capacity in separating and thus classifying data populations. Resource classification is a typical activity in the mining industry. There are some documented international codes, which have been developed in practice, for classification of mineral resource. However, many of such codes are not enforcement tools. The JORC is one of the codes that is most widely used for provision of information that is exhaustive and broadly in accordance with mining companies' objectives. The JORC classifies mineral resources as measured, indicated and inferred depending on the degrees of confidence. Ore reserves can be classified as proven and probable from either measured or indicated mineral resource. Converting from mineral resource to ore reserve depending on the modifying factor such as mining, processing, metallurgical, infrastructure, economic, marketing, legal, environment, social, government and particularly on the final decision of a competent person (JORC, 2012).

In this research, the aim was to introduce an innovative technique, which is based on the combination of geostatistical simulation and fractal modeling, for mineral resource classification. Conventional methods of interpolation have been established based on geostatistical techniques like kriging, which leads to biased estimation on the basis of smoothing effect and, thus, unreliable decisions. As described earlier, quantification of uncertainty in global and local and spatial scales can be achieved by conditional Gaussian simulation. The generated realizations are amenable to resource and reserve classifications, and one cannot see any smoothness as compared to kriging results. The mineral resource classification is thus more reliable with geostatistical simulation. Interestingly, the SS–N technique yields more reliable information of mineralized zones, as they are more consistent with grade distribution since each realization reproduces the supposed histogram of declustered data. Mineralized zones are then classified into measured, indicated and inferred resources (Table 4). The tonnage-cut-off curve is also calculated to highlight the difference between the methods. From Fig. 15, it can be seen the biased effect from the C–V model.

4. Conclusions

Orebody modeling is the most important stage in mine planning and risk analysis. Classification of mineral resource is complicated but should be consistent with geological interpretation. Compared to existing methods of mineral resource classification, this new technique can deal with the complexity of the data yet produces reliable results for

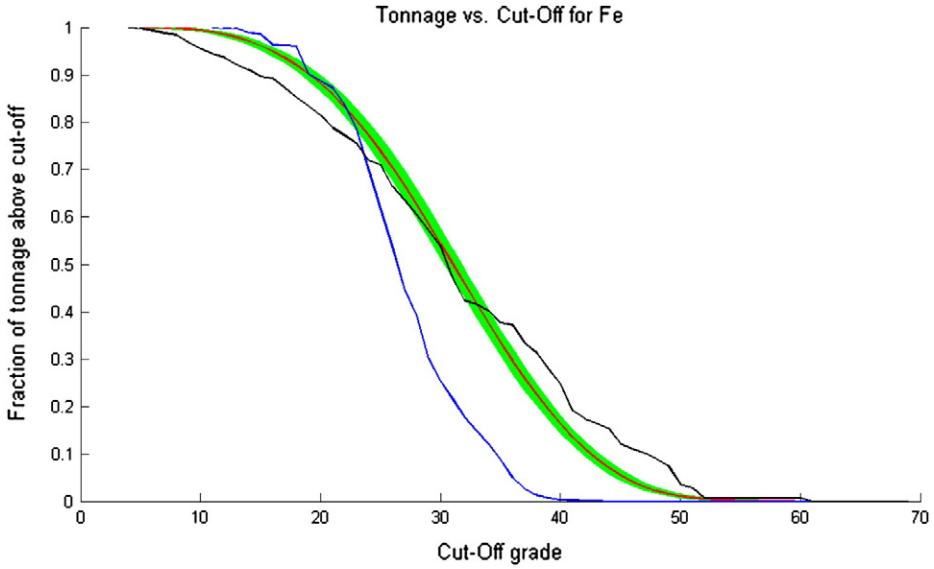

Fig. 15. Tonnage-cut-off curves. Green: individual realizations. Red: average of realizations (SS–N). Blue: C–V model. Black: Global (N–S) model.

different parts of a mineral deposit. Fractal modeling is highly critical for delineation of mineralized zones, and can be proposed for estimation of mineral resources. In this paper, the proposed SS–N technique is an attempt to combine the fractal modeling (S–N) with geostatistical simulation. Therefore, the application of the C–V model, which uses interpolated data (in this study, by kriging), leads to less reliable estimates. The proposed SS–N technique yields (i) robust log–log plots for realizations obtained from geostatistical simulation and (ii) more reliable mineral resource estimates of the Fe grade in the Zaghia deposit. The proposed SS–N technique can be used as a substitute for conventional methods of modeling and estimation of ore deposits. This proposed technique, SS–N, is applicable when there is no geological information for constructing the estimation domains.

Acknowledgments

The authors would like to thank Prof. Xavier Emery for permission to use the related computer program, Mr. Mojtaba Shahidipour for his worthwhile assistance in language editing, the editor (Prof. Renguang Zuo) and anonymous reviewers of this paper for their comments and valuable remarks.

Appendix A

Programming was done in MATLAB 2008 environment since its capability in drawing log–log plots, and also generating the average over the realizations.

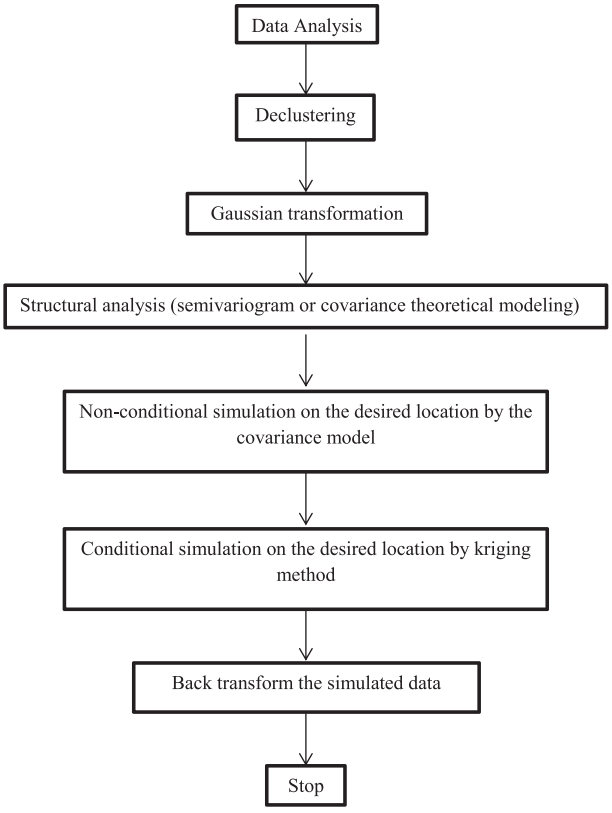

Appendix B. Supplementary data

Supplementary data to this article can be found online at http://dx.doi.org/10.1016/j.gexplo.2014.11.007.

```
for j=1:100
a= sort(data(:,j),'descend');
for i=1:size(a,1)
    a(i,2)=sum(a(:,1)==a(i,1));
end
a(1,3)=a(1,2);
for i=2:size(a,1)
    a(i,3)=a(i,2)+a((i-1),3);
end

a(:,4)=log10(a(:,1));
a(:,5)=log10(a(:,3));
frac(:,j)=a(:,5);

hold on
figure(1);
plot(a(:,4),a(:,5),'.');
f=min(a(:,4))-0.5;
g=(max(a(:,4))+0.5);
h=min(a(:,5))-0.5;
n=max(a(:,5))+0.5;
xlabel('Log Fe');
ylabel('Log No.');
title('Fractal Method-(SS-N)');
grid on

end
```

References

Afzal, P., Khakzad, A., Moarefvand, P., Rashidnejad Omran, N., Esfandiari, B., Fadakar Alghalandis, Y., 2010. Geochemical anomaly separation by multifractal modeling in Kahang (Gor Gor) porphyry system, Central Iran. J. Geochem. Explor. 104, 34–46.

Afzal, P., Fadakar Alghalandis, Y., Khakzad, A., Moarefvand, P., Rashidnejad Omran, N., 2011. Delineation of mineralization zones in porphyry Cu deposits by fractal concentration–volume modeling. J. Geochem. Explor. 108, 220–232.

Afzal, P., Fadakar Alghalandis, Y., Moarefvand, P., Rashidnejad Omran, N., Asadi Haroni, H., 2012. Application of power–spectrum–volume fractal method for detecting hypogene, supergene enrichment, leached and barren zones in Kahang Cu porphyry deposit, Central Iran. J. Geochem. Explor. 112, 131–138.

Agterberg, F.P., 1995. Multifractal modelling of the sizes and grades of giant and supergiant deposits. Int. Geol. Rev. 37, 1–8.

Agterberg, F.P., Cheng, Q., Wright, D.F., 1993. Fractal modeling of mineral deposits. In: Elbrond, J., Tang, X. (Eds.), 24th APCOM Symposium Proceeding, Montreal, Canada, pp. 43–53.

Agterberg, F.P., Cheng, Q., Brown, A., Good, D., 1996. Multifractal modeling of fractures in the Lac du Bonnet Batholith, Manitoba. Comput. Geosci. 22, 497–507.

Ahrens, L.H., 1954a. The lognormal distribution of the elements (a fundamental law of geochemistry and its subsidiary). Geochim. Cosmochim. Acta 5, 49–73.

Ahrens, L.H., 1954b. The lognormal distribution of the elements II. Geochim. Cosmochim. Acta 6, 121–131.

Ahrens, L.H., 1966. Element distributions in specific igneous rocks—VIII. Geochim. Cosmochim. Acta 30, 109–122.

Ali, K., Cheng, Q., Chen, Z., 2007. Multifractal power spectrum and singularity analysis for modelling stream sediment geochemical distribution patterns to identify anomalies related to gold mineralization in Yunnan Province, South China. Geochem. Explor. Environ. Anal. 7, 293–301.

Armstrong, M., Boufassa, A., 1988. Comparing the robustness of ordinary kriging and lognormal kriging: outlier resistance. Math. Geol. 20 (4), 447–457.

Bai, J., Porwal, A., Hart, C., Ford, A., Yu, L., 2010. Mapping geochemical singularity using multifractal analysis: application to anomaly definition on stream sediments data from Funin Sheet, Yunnan, China. J. Geochem. Explor. 104, 1–11.

Bolviken, B., Stokke, P.R., Feder, J., Jossang, T., 1992. The fractal nature of geochemical landscapes. J. Geochem. Explor. 43, 91–109.

Brooker, P.I., 1985. Two-dimensional simulation by turning bands. Math. Geol. 17 (1), 81–90.

Carranza, E.J.M., 2009. Geochemical anomaly and mineral prospectivity mapping in GIS. Handbook of Exploration and Environmental Geochemistry. 11. Elsevier, Amsterdam.

Carranza, E.J.M., 2010a. Catchment basin modelling of stream sediment anomalies revisited: incorporation of EDA and fractal analysis. Geochem. Explor. Environ. Anal. 10, 365–381.

Carranza, E.J.M., 2010b. Mapping of anomalies in continuous and discrete fields of stream sediment geochemical landscapes. Geochem. Explor. Environ. Anal. 10, 171–187.
Carranza, E.J.M., 2011a. Analysis and mapping of geochemical anomalies using logratio-transformed stream sediment data with censored values. J. Geochem. Explor. 110, 167–185.
Carranza, E.J.M., 2011b. From predictive mapping of mineral prospectivity to quantitative estimation of number of undiscovered prospects. Resour. Geol. 61, 30–51.
Carranza, E.J.M., Sadeghi, M., 2010. Predictive mapping of prospectivity and quantitative estimation of undiscovered VMS deposits in Skellefte district (Sweden). Ore Geol. Rev. 38, 219–241.
Carranza, E.J.M., Owusu, E., Hale, M., 2009. Mapping of prospectivity and estimation of number of undiscovered prospects for lode–gold, southwestern Ashanti Belt, Ghana. Mineral. Deposita 44 (8), 915–938.
Cheng, Q., 2007. Mapping singularities with stream sediment geochemical data for prediction of undiscovered mineral deposits in Gejiu, Yunan Province, China. Ore Geol. Rev. 32, 314–324.
Cheng, Q., Agterberg, F.P., Ballantyne, S.B., 1994. The separation of geochemical anomalies from background by fractal methods. J. Geochem. Explor. 51, 109–130.
Chentsov, N.N., 1957. Levy Brownian motion for several parameters and generalized white noise. Theory Probab. Appl. 2, 265–266.
Chilès, J.P., 1977. Géostatistique des phénoménes non stationnaires (dans le plan), doctoral thesis. Université de Nancy I, Nancy (152 pp.).
Chilès, J.P., Delfiner, P., 2012. Geostatistics: Modeling Spatial Uncertainty. Wiley, New York.
Clark, I., 1999. A case study in the application of geostatistics to lognormal and quasi-lognormal problems. 28th International Symposium on Application of Computers and Operations Research in the Mineral Industry. Colorado School of Mines, CSM, pp. 407–416.
Daneshvar Saein, L., Rasa, I., Rashidnejad Omran, N., Moarefvand, P., Afzal, P., Sadeghi, B., 2013. Application of number–size (N–S) fractal model to quantify of the vertical distributions of Cu and Mo in Nowchun porphyry deposit (Kerman, SE Iran). Arch. Min. Sci. 58 (1), 89–105.
David, M., 1977. Geostatistical Ore Reserve Estimation. Elsevier, Amsterdam.
Davis, J.C., 2002. Statistics and Data Analysis in Geology. 3rd ed. John Wiley & Sons Inc, New York.
Delhomme, J.P., 1979. Spatial variability and uncertainty in groundwater flow parameters: a geostatistical approach. Water Resour. Res. 15, 269–280.
Deng, J., Wang, Q., Yang, L., Wang, Y., Gong, Q., Liu, H., 2010. Delineation and explanation of geochemical anomalies using fractal models in the Heqing area, Yunnan Province, China. J. Geochem. Explor. 105, 95–105.
Deutsch, C.V., Journel, A.G., 1998. GSLIB: Geostatistical Software Library and User's Guide. Oxford University Press, New York.
Emery, X., 2004. Testing the correctness of the sequential algorithm for simulating Gaussian random fields. Stoch. Env. Res. Risk A. 18 (6), 401–413.
Emery, X., 2005. Simple and ordinary kriging multiGaussian kriging for estimating recoverable reserves. Math. Geol. 37, 295–319.
Emery, X., 2008. A turning bands program for conditional co-simulation of cross-correlated Gaussian random fields. Comput. Geosci. 34, 1850–1862.
Emery, X., 2012. Co-simulating total and soluble copper grades in an oxide ore deposit. Math. Geosci. 44 (1), 27–46.
Emery, X., González, K.E., 2007. Probabilistic modelling of mineralogical domains and its application to resources evaluation. J. S. Afr. Inst. Min. Metall. 107 (12), 803–809.
Emery, X., Lantuejoul, C., 2006. TBSIM: a computer program for conditional simulation of three-dimensional Gaussian random fields via the turning bands method. Comput. Geosci. 32, 1615–1628.
Emery, X., Robles, L.N., 2009. Simulation of mineral grades with hard and soft conditioning data: application to a porphyry copper deposit. Comput. Geosci. 13 (1), 79–89.
Emery, X., Bertini, J.P., Ortiz, J.M., 2005. Resource and reserve evaluation in the presence of imprecise data. CIM Bull. 98 (1089) (12 pp.).
Emery, X., Ortiz, J.M., Rodríguez, J.J., 2006. Quantifying uncertainty in mineral resources by use of classification schemes and conditional simulations. Math. Geol. 38 (4), 445–464.
Gneiting, T., 1998. Closed form solutions of the two-dimensional turning bands equation. Math. Geol. 30 (4), 379–390.
Goncalves, M.A., Mateus, A., Oliveira, V., 2001. Geochemical anomaly separation by multifractal modeling. J. Geochem. Explor. 72, 91–114.
Hassanpour, S., Afzal, P., 2011. Application of concentration–number (C–N) multifractal modeling for geochemical anomaly separation in Haftcheshmeh porphyry system, NW Iran. Arab. J. Geosci. 6 (3), 957–970.
He, J., Yao, S., Zhang, Z., You, G., 2013. Complexity and productivity differentiation models of metallogenic indicator elements in rocks and supergene media around Daijiazhuang Pb–Zn deposit in Dangchang County, Gansu Province. Nat. Resour. Res. 22, 19–36.
Houlding, S.W., 2000. Practical Geostatistics: Modeling and Spatial Analysis. Germany, Springer, Berlin.
International minerals engineering consultant Co. (IMECCO), 2010. General Exploration of Zaghia (IIC) Iron Ore Deposit Report. Iran Minerals Production & Supply Co. (IMPASCO).
JORC, 2012. Australasian code for reporting of exploration results, mineral resources and ore reserves. Report Prepared by the Joint Ore Reserve Committee of the Australasian Institute of Mining andMetallurgy, Australian Institute of Geoscientists and Minerals Council of Australia, the JORC Code, 2012 edition (44 pp.).
Journel, A.G., 1983. Nonparametric estimation of spatial distribution. Math. Geol. 15 (3), 445–468.
Journel, A.B., Huijbregts, C.J., 1978. Mining Geostatistics. Academic, New York.
Lantuejoul, C., 2002. Geostatistical Simulation. Models and Algorithms, Springer, Berlin.
Li, C., Xu, Y., Jiang, X., 1994. The fractal model of mineral deposits. Geol. Zhejiang 10 (25), 25–32 (In Chinese with English Abstract).
Li, C., Ma, T., Shi, J., 2003. Application of a fractal method relating concentrations and distances for separation of geochemical anomalies from background. J. Geochem. Explor. 77, 167–175.
Limpert, E., Stahel, W.A., Abbt, M., 2001. Lognormal distributions across the sciences: keys and clues. Bioscience 51 (5), 341–352.
Luz, F., Mateus, A., Matos, J.X., Gonçalves, M.A., 2014. Cu- and Zn-soil anomalies in the NE Border of the South Portuguese Zone (Iberian Variscides, Portugal) identified by multifractal and geostatistical analyses. Nat. Resour. Res. 23, 195–215.
Maleki Tehrani, M.A., Asghari, O., Emery, X., 2013. Simulation of mineral grades and classification of mineral resources by using hard and soft conditioning data: application to Sungun porphyry copper deposit. Arab. J. Geosci. 6 (10), 3773–3781.
Mandelbrot, B.B., 1983. The Fractal Geometry of Nature. W. H. Freeman, San Fransisco.
Mantoglou, A., Wilson, J.L., 1982. The turning bands method for simulation of random fields using line generation by a spectral method. Water Resour. Res. 18, 1379–1394.
Matheron, G., 1973. The intrinsic random functions and their applications. Adv. Appl. Probab. 5 (3), 439–468.
Matheron, G., 1989. Estimating and choosing: an essay on probability in practice. Springer-Verlag, Berlin (141 pp.).
Monecke, T., Gemmell, J.B., Monecke, J., 2001. Fractal distributions of veins in drill core from the Hellyer VHMS deposit. Australia: constraints on the origin and evolution of the mineralising system. Miner. Deposita 36, 406–415.
Monecke, T., Monecke, J., Herzig, P.M., Gemmell, J.B., Monch, W., 2005. Truncated fractal frequency distribution of element abundance data: a dynamic model for the metasomatic enrichment of base and precious metals. Earth Planet. Sci. Lett. 232, 363–378.
Montoya, C., Emery, X., Rubio, E., Wiertz, J., 2012. Multivariate resources modelling for assessing uncertainty in mine design and mine planning. J. S. Afr. Inst. Min. Metall. 112, 353–363.
Nazarpour, A., Sadeghi, B., Sadeghi, M., 2015. Application of fractal models to characterization and evaluation of vertical distribution of geochemical data in Zarshuran gold deposit, NW Iran. J. Geochem. Explor. 148, 60–70.
Nouri, R., Jafari, M.R., Arian, M., Feizi, F., Afzal, P., 2013. Correlation between Cu mineralization and major faults using multifractal modelling in the Tarom area (NW Iran). Geol. Carpath. 64 (5), 409–416.
Ortiz, J.M., Emery, X., 2006. Geostatistical estimation of mineral resources with soft geological boundaries: a comparative study. J. S. Afr. Inst. Min. Metall. 106 (8), 577–584.
Ramezani, J., Tucker, R.D., 2003. The Saghand region, Central Iran: U–Pb geochronology, petrogenesis and implications for Gondwana tectonics. Am. J. Sci. 303, 622–665.
Razumovsky, N., 1940. Distribution of metal values in ore deposits. C. R. Acad. Sci. l'URSS 9, 814–816.
Reimann, C., Filzmoser, P., 2000. Normal and lognormal data distribution in geochemistry: death of a myth. Consequences for the statistical treatment of geochemical and environmental data. Environ. Geol. 39, 1001–1014.
Rossi, M., Deutsch, C., 2014. Mineral resource estimation. Springer, New York.
Sadeghi, B., Moarefvand, P., Afzal, P., 2011. Determination of Fe grade distribution by using of concentration–number fractal method in boreholes of Zaghia iron ore deposit, Bafq. Earth Resour. J. 3, 51–60 (In Persian with English abstract).
Sadeghi, B., Moarefvand, P., Afzal, P., Yasrebi, A.B., Daneshvar Saein, L., 2012. Application of fractal models to outline mineralized zones in the Zaghia iron ore deposit, Central Iran. J. Geochem. Explor. 122, 9–19 (Special Issue "fractal/multifractal modelling of geochemical data").
Sanderson, D.J., Zhang, X., 1999. Critical stress localization of flow associated with deformation of well-fractured rock masses, with implications for mineral deposits.Geological Society, London. Special Publications 155, 69–81.
Sanderson, D.J., Roberts, S., Gumiel, P., 1994. A Fractal relationship between vein thickness and gold grade in drill core from La Codosera, Spain. Econ. Geol. 89, 168–173.
Shen, W., Zhao, P., 2002. Theoretical study of statistical fractal model with applications to mineral resource prediction. Comput. Geosci. 28, 369–376.
Shi, J., Wang, C., 1998. Fractal analysis of gold deposits in China: implication for giant deposit exploration. Earth Sci. J. China Univ. Geosci. 23, 616–618 (In Chinese with English Abstract).
Shinozuka, M., Jan, C.M., 1972. Digital simulation of random processes and its applications. J. Sound Vib. 25, 111–128.
Sim, B.L., Agterberg, F.P., Beaudry, C., 1999. Determining the cut off between background and relative base metal contamination levels using multifractal methods. Comput. Geosci. 25, 1023–1041.
Spalla, M.I., Morotta, A.M., Gosso, G., 2010. Advances in Interpretation of Geological Processes: Refinement of Multi-scale Data and Integration in Numerical Modeling. Geological Society, London.
Turcotte, D.L., 1986. A fractal approach to the relationship between ore grade and tonnage. Econ. Geol. 18, 1525–1532.
Turcotte, D.L., 1996. Fractals and Chaos in Geophysics. 2nd ed. Cambridge University Press, Cambridge UK, pp. 81–99.
Turcotte, D.L., 2002. Fractals in petrology. Lithos 65, 261–271.
Wang, Z., Cheng, Q., 2006. Characterization of micro-texture of quartz mylonite deformation process using fractal P–A model. Earth Sci. J. China Univ. Geosci. 31 (3), 361–365 (in Chinese with English Abstract).
Wang, Z., Cheng, Q., Cao, L., 2007. Fractal modeling of the microstructure property of quartz mylonite during deformation process. Math. Geol. 39, 53–68.
Wang, Z., Cheng, Q., Xu, D., Dong, Y., 2008. Fractal modeling of sphalerite banding in jinding Pb–Zn deposit, Yunnan, southwestern China. J. China Univ. Geosci. 19, 77–84.
Wang, Q., Deng, J., Liu, H., Yang, L., Wan, L., Zhang, R., 2010a. Fractal models for ore reserve estimation. Ore Geol. Rev. 37, 2–14.

Wang, Q., Deng, J., Zhao, J., Liu, H., Wan, L., Yang, L., 2010b. Tonnage-cutoff model and average grade-cutoff model for a single ore deposit. Ore Geol. Rev. 38, 113–120.
Wang, Q., Deng, J., Liu, H., Wang, Y., Sun, X., Wan, L., 2011. Fractal models for estimating local reserves with different mineralization qualities and spatial variations. J. Geochem. Explor. 108, 196–208.
Wang, G., Carranza, E.J.M., Zuo, R., Hao, Y., Du, Y., Pang, Z., Sun, Y., Qu, J., 2012. Mapping of district-scale potential targets using fractal models. J. Geochem. Explor. 122, 47–54.
Wang, G., Pang, Z., Boisvert, J.B., Hao, Y., Cao, Y., Qu, J., 2013. Quantitative assessment of mineral resources by combining geostatistics and fractal methods in the Tongshan porphyry Cu deposit (China). J. Geochem. Explor. 134, 85–98.
Wilson, C.E., Aydin, A., Durlofsky, L.J., Boucher, A., Brownlow, D., 2011. Use of outcrop observations, geostatistical analysis, and flow simulation to investigate structural controls on secondary hydrocarbon migration in the Anacacho limestone, Uvalde, Texas. AAPG Bull. 95 (7), 1181–1206.
Zhang, Z., Mao, H., Cheng, Q., 2001. Fractal geometry of element distribution on mineral surface. Math. Geol. 33 (2), 217–228.
Zuo, R., Cheng, Q., Xia, Q., 2009. Application of fractal models to characterization of vertical distribution of geochemical element concentration. J. Geochem. Explor. 102, 37–43.
Zuo, R., Carranza, E.J.M., Cheng, Q., 2012. Fractal/multifractal modelling of geochemical exploration data. J. Geochem. Explor. 122, 1–3.
Zuo, R., Xia, Q., Zhang, D., 2013. A comparison study of the C–A and S–A models with singularity analysis to identify geochemical anomalies in covered areas. Appl. Geochem. 33, 165–172.
Zuo, R., Wang, J., Chen, G., Yang, M., 2015. Identification of weak anomalies: a multifractal perspective. J. Geochem. Explor. 148, 12–24.